

***Ab initio* Picture of Nuclei: Shapes, Rotations, and Vibrations from Chiral Potentials**

**K.D. Launey¹, A.C. Dreyfuss^{1,2}, G.H. Sargsyan¹, R.B. Baker¹,
M. Miora¹, J.P. Draayer¹, T. Dytrych^{1,3}**

¹Dept. of Physics & Astronomy, Louisiana State University, LA 70803, USA

²Lawrence Livermore National Laboratory, Livermore, California 94550, USA

³Nuclear Physics Institute, 250 68 Řež, Czech Republic

Received 3 November 2017

Abstract. The *ab initio* symmetry-adapted no-core shell model is a first-principle framework, which can now expand the reach of the *ab initio* theory, by exploiting approximate symmetries found to dominate in atomic nuclei, namely, the deformation related SU(3) and its embedding symplectic Sp(3,R) symmetry. This allows one to achieve nuclear descriptions, including the emergence of collective modes and α -capture reactions, starting from the properties of two or three nucleons often tied to the symmetry patterns of quark and gluon dynamics. Furthermore, one can utilize the symplectic Sp(3,R) symmetry to identify equilibrium deformation, rotational bands and giant-resonance modes.

1 Introduction

Many successful models developed over the last several decades have improved our understanding of the atomic nucleus. However, the complex nature of nuclear dynamics remains a challenge with subtle nuclear features still not completely understood. An ideal framework to study the physics of atomic nuclei is the *ab initio* theory [1–13], or from first principles. This, coupled with high performance computing (HPC), can inform us – without *a priori* assumptions of the degrees of freedom – about strongly interacting systems based on the nature of the strong force and of the way this force governs the structure and reactions of nuclei. And while nuclei are intricate many-particle quantum mechanical systems with non-perturbative inter-nucleon interactions, observations have revealed that they often display striking simplicities; for example, experimental evidence supports formation of enhanced deformation and clusters, as well as vibrational and rotational patterns, as suggested by energy spectra, electric monopole and quadrupole transitions, radii and quadrupole moments [14, 15]. Symmetries underpin orderly patterns, and it has been earlier recognized that the highly structured patterns observed in low-lying nuclear states might be understood by the symplectic Sp(3, \mathbb{R}) symmetry [15–17]. In this article, we report on our findings deduced from first-principle investigations, namely, we now understand that nuclei exhibit comparatively simple physics in their low-lying states

governed by the $\text{Sp}(3, \mathbb{R})$ symmetry, which together with its slight symmetry breaking naturally describes atomic nuclei, including deformation, rotations, vibrations, and shape coexistence.

2 Simple Pattern Formation from First Principles – Role of the Symplectic $\text{Sp}(3, \mathbb{R})$ Symmetry

The symplectic $\text{Sp}(3, \mathbb{R})$ symmetry and its deformation-related $\text{SU}(3)$ subgroup underpin the symplectic model [16, 17, 20], the fully microscopic no-core symplectic shell model (NCSpM) [21–23], and the *ab initio* symmetry-adapted no-core shell model (SA-NCSM) [10, 24]. Both symmetries have been found to play a key role across the nuclear chart – from the lightest systems of ${}^6\text{Li}$, ${}^8\text{Be}$, ${}^{12}\text{C}$, and ${}^{16}\text{O}$ [10, 21–23, 25], through intermediate-mass (*sd*-shell) nuclei [24, 26, 27], up to strongly deformed nuclei of the rare-earth and actinide regions [17, 28, 29]. That $\text{SU}(3)$ plays a key role tracks with the seminal work of Elliott [19, 30, 31], where only a few dominant $\text{SU}(3)$ configurations have been observed in many nuclei even in the case of a symmetry-breaking interaction (see, e.g., Figure 1). The $\text{SU}(3)$ -symmetry dominance has been also observed in heavier nuclei, where pseudo-spin symmetry and its pseudo- $\text{SU}(3)$ complement have been shown to play a similar role in accounting for deformation in the upper *pf* and lower *sdg* shells, and in particular, in strongly deformed nuclei of the rare-earth and actinide regions [32], as well as in many other studies (e.g., [33]).

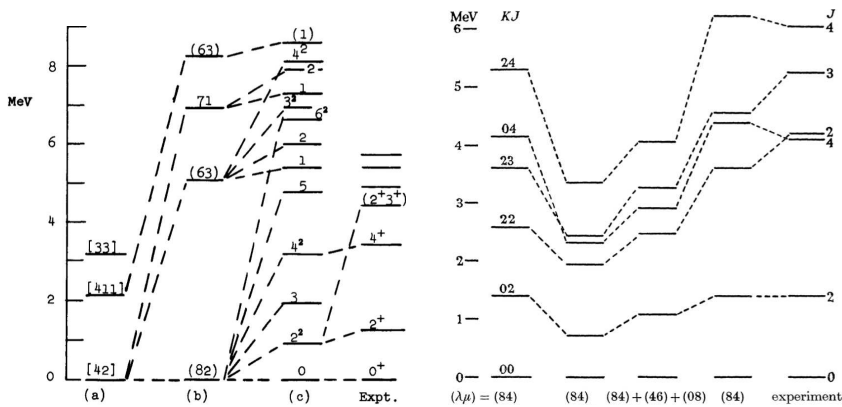


Figure 1. Elliott’s $\text{SU}(3)$ model applied to *sd*-shell nuclei. Left panel: Spectrum of ${}^{22}\text{Ne}$ (a) with a Majorana potential, (b) with the addition of the second-order $\text{SU}(3)$ Casimir invariant, C_2^{su3} , and (c) with the Majorana potential plus an attractive $Q \cdot Q$ interaction [or (b) with the addition of L^2]. Figure taken from [18]. Right panel: Spectrum of ${}^{24}\text{Mg}$ with a Gaussian central force. Figure taken from [19]. The vertical axis in both figures represents energy in MeV. Note the importance of the most deformed $\text{SU}(3)$ configuration (8 2) in ${}^{22}\text{Ne}$ and (8 4) in ${}^{24}\text{Mg}$ for reproducing the experimental low-lying states.

The symplectic $\text{Sp}(3, \mathbb{R})$ symmetry, in turn, is an important symmetry of atomic nuclei that can be understood to naturally describe rotations and vibrations of equilibrium deformation [20].

The *ab initio* SA-NCSM capitalizes on exact as well as partial symmetries that underpin the structure of nuclei and provides remarkable insight into how simple symmetry patterns emerge in the many-body nuclear dynamics from first principles [24]. It adopts the first-principle concept and utilizes many-particle basis states that are organized with respect to the physically relevant, deformation-related $\text{SU}(3)_{(\lambda\mu)} \supset \overset{\kappa}{\text{SO}}(3)_L$ subgroup chain (for reviews, see [24, 34]), that is, it is a no-core shell model with $\text{SU}(3)$ -coupled basis states (hence, the SA-NCSM results obtained in a complete N_{max} space are equivalent to the N_{max} NCSM results). In this basis, the full model space can be down-selected to the physically relevant space using considerations based on the symplectic $\text{Sp}(3, \mathbb{R})$ symmetry.

The *ab initio* SA-NCSM results for p -shell nuclei reveal a dominance of configurations of large deformation in the $0\hbar\Omega$ subspace. For example, the *ab initio* $N_{\text{max}} = 10$ SA-NCSM results with the bare JISP16 realistic interaction [35] (similarly, for the bare N^3LO realistic interaction [36]) for the ${}^6\text{Li}$ 1^+ ground state (*g.st.*) and its rotational band reveal the dominance of the leading $0\hbar\Omega$ (2 0) irreducible representation (irrep) and its symplectic excitations (Figure 2). Furthermore, as illustrated in Figure 2 by a red arrow, the ${}^6\text{Li}$ ground state projects at the 80% level onto a single symplectic irrep, implying a predominance of a single equilibrium shape, described by the $\text{SU}(3)$ $0\hbar\Omega$ (2 0) configuration (beginning of the red arrow in Figure 2), with vibrations induced by the monopole \hat{r}^2 ($L = 0$) and quadrupole \hat{Q} ($L = 2$) operators and described by multi-particle-multi-hole (mp - mh) $\text{SU}(3)$ configurations (traced by the red arrow in Figure 2) extended up to 10p-10h excitations. This is also observed for, e.g., ${}^6\text{He}$, ${}^8\text{Be}$, ${}^{12}\text{C}$, and ${}^{16}\text{O}$. The outcome points to a remarkable feature common to the low-lying states of nuclei that has heretofore gone unrecognized in other first-principle studies; namely, the emergence, without a priori constraints, of simple orderly patterns that favor strongly deformed configurations and low spin values. This feature confirms the dominant role the $\text{SU}(3)$ and $\text{Sp}(3, \mathbb{R})$ symmetries play in nuclear dynamics and is central to expanding the reach of first-principle studies to heavier nuclei [37]. In particular, this supports a *symmetry-guided* model space selection, which implies inclusion of the full space up through N_{max}^{\perp} , and a subset of deformation/spin configurations beyond this, up through N_{max}^{\top} , labeled as $\langle N_{\text{max}}^{\perp} \rangle N_{\text{max}}^{\top}$ and symbolically illustrated in Figure 2. This allows the SA-NCSM to advance an extensible microscopic framework for studying nuclear structure and reactions that capitalizes on advances being made in *ab initio* methods while exploiting symmetries found to dominate the dynamics.

Utilizing the symmetry-guided concept, *ab initio* calculations for intermediate-mass nuclei become feasible. For example, Figure 2 and Table 1 show the lowest

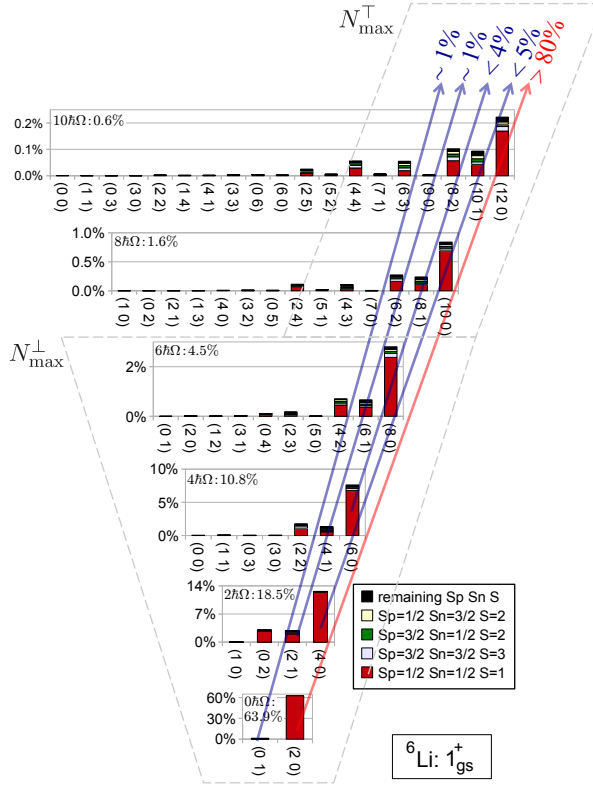


Figure 2. (color online) Probability distributions for proton, neutron, and total intrinsic spin components (S_p, S_n, S) across the Pauli-allowed deformation-related ($\lambda\mu$) values for the 1^+ ground state of ${}^6\text{Li}$, calculated in 12 HO shells with the JISP16 bare interaction ($\hbar\Omega = 20$ MeV). The concentration of strengths to the far right demonstrates the dominance of collectivity. The projection onto symplectic irreps (with probability $\geq 1\%$) is schematically illustrated for ${}^6\text{Li}$ by arrows and clearly reveals the preponderance of a single symplectic irrep (vertical cone). Figure adapted from Ref. [10].

five 0^+ states and the lowest seven 2^+ states in ${}^{18}\text{Ne}$, calculated in the *ab initio* SA-NCSM, with the dominant $\text{SU}(3)$ configurations listed in Table 1. Each of these configurations for the states below 20 MeV peaks at a $0p\text{-}0h$ configuration, which – being the beginning of a symplectic vertical cone – describes an equilibrium shape, with vibrations of this shape extended to higher particle-hole excitations. Note that the third excited 0^+ state is a $2\hbar\Omega$ $2p\text{-}2h$ configuration describing a shape considerably more deformed than the ground state, while the $2\hbar\Omega$ $1p\text{-}1h$ vibration of the ground state (same shape) appears as the giant monopole resonance around 30 MeV.

Ab Initio Picture of Nuclei: Shapes, Rotations, and Vibrations

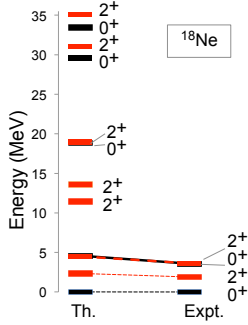


Figure 3. (color online) SA-NCSM calculations with chiral potentials for ^{18}Ne in the ultra-large model space of 9 shells. Simulations use the NNLO_{opt} NN interaction [38] and $\hbar\Omega = 15$ MeV, and are performed on the Blue Waters system.

Table 1. Probability amplitudes of the dominant $(\lambda\mu)$ S configurations for the ^{18}Ne lowest 0^+ and 2^+ states shown in the order they appear in Figure 2 according to their excitation energy. The dominant modes are identified by the corresponding symplectic irreps for the configurations underlined. The SA-NCSM calculations use the NNLO_{opt} NN interaction [38] and $\hbar\Omega = 15$ MeV.

	$0\hbar\Omega$ $0p$ - $0h$			$2\hbar\Omega$		Dominant mode
	$(4\ 0)$ $S = 0$	$(0\ 2)$ $S = 0$	$(2\ 1)$ $S = 1$	$(8\ 2)$ $S = 0$	$(6\ 0)^*$ $S = 0$	
$0^+_{\text{g.st.}}$	<u>0.43</u>	0.16	0.10			prolate shape
2^+	<u>0.33</u>	0.16	0.21			prolate shape
0^+	0.19	<u>0.45</u>	0.02			oblate shape
2^+	0.23	<u>0.30</u>	0.16			oblate shape
2^+	0.05	<u>0.08</u>	<u>0.56</u>			prolate shape ($S=1$)
2^+	0.05	0.07	<u>0.54</u>			prolate shape ($S=1$)
0^+	0.03	0.07	<u>0.54</u>			prolate shape ($S=1$)
2^+	0.02	0.07	<u>0.57</u>			prolate shape ($S=1$)
0^+				<u>$\hat{E}0.47$</u>		large prolate shape (2p-2h)
2^+				<u>$\hat{E}0.47$</u>		large prolate shape (2p-2h)
0^+					<u>$\hat{E}0.44$</u>	giant monopole resonance (1p-1h)
2^+					<u>$\hat{E}0.46$</u>	giant quadrupole resonance (1p-1h)

*Part of the symplectic irrep (vertical cone) that starts at $0\hbar\Omega$ $(4\ 0)$ $S = 0$ and dominates in the $0^+_{\text{g.st.}}$ ground state together with its 2^+ rotation.

3 The Elusive Hoyle State and Negative-Parity States in ^{12}C

The Hoyle state was predicted based on observed abundances of heavy elements in the universe [39] and has attracted much recent attention both in theory (e.g., see [8, 40, 41]) and experiment (e.g., [42–44]). The findings of the NCSpM inform key features of the primary physics responsible for the emergent phenomena of large deformation and alpha-cluster substructures in ^8Be and ^{12}C [21, 45], as well as enhanced collectivity in intermediate-mass nuclei, such as ^{20}O , $^{20,22,24}\text{Ne}$, $^{20,22}\text{Mg}$, and ^{24}Si [22] (Figure 4).

The NCSpM is a fully microscopic no-core shell model that can be employed in

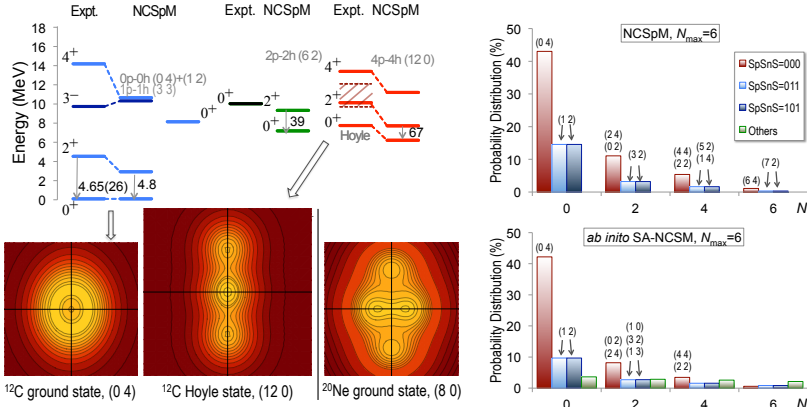


Figure 4. (color online) Left: ^{12}C energy spectrum (in MeV) and $B(E2)$ rates (in W.u.) calculated by the NCSpM using the schematic interaction of Eq. (1) with the bare JISP16 NN and 5 symplectic irreps (shown above each band) expanded up to $N_{\text{max}} = 20$, and compared to experiment (“Expt.”) [46]. One-body density profiles *in the intrinsic frame* reveal a torus-like shape for the ^{12}C 0_{gs}^+ and overlapping clusters in the Hoyle state. Right: Probability distribution across total HO quanta excitations for the ^{12}C 0_{gs}^+ – close similarity is observed for NCSpM (top) and SA-NCSM (bottom) for $N_{\text{max}} = 6$ and $\hbar\Omega = 18$ MeV [21]. Dominant ($\geq 1\%$) SU(3) modes are also shown. Very similar results are obtained for 2_1^+ and 4_1^+ [23].

model spaces beyond current NCSM limits. It uses a symplectic $\text{Sp}(3, \mathbb{R})$ basis but is not limited to $\text{Sp}(3, \mathbb{R})$ -preserving interactions. The NCSpM employed within a full model space up through a given N_{max} coincides with the NCSM for the same N_{max} cutoff. However, in the case of the NCSpM, the symplectic irreps divide the space into ‘vertical cones’ that are comprised of basis states of a definite deformation ($\lambda\mu$). Hence, the model space can be reduced to only a few important configurations that are chosen among all possible $\text{Sp}(3, \mathbb{R})$ irreps within the N_{max} model space. We employ a Hamiltonian with an effective interaction derived from the long-range expansion of the two-body central nuclear force,

$$H_{\text{eff}} = H_0 + \frac{\chi}{2} \frac{(e^{-\gamma Q \cdot Q} - 1)}{\gamma} + V_{NN}^{\text{SB}}, \quad (1)$$

where V_{NN}^{SB} is a symmetry-breaking term applied to symplectic bandheads (we adopt either a spin-orbit term, $-\kappa \sum_{i=1}^A l_i \cdot s_i$ [21, 23], or a realistic interaction [46], such as the bare interactions, JISP16 [35] or chiral N3LO [36] NN). The $\text{Sp}(3, \mathbb{R})$ -preserving part of the Hamiltonian includes: the total kinetic energy plus the spherical HO potential (H_0), and the important $\frac{1}{2} Q \cdot Q = \frac{1}{2} \sum_s q_s \cdot (\sum_t q_t)$ interaction, which realizes the physically relevant interaction of each particle with the total quadrupole moment of the nuclear system (for a valence

shell and very small γ , the Elliott model is recovered). The considerable average contribution, $\langle Q \cdot Q \rangle$, of $Q \cdot Q$ is removed [47]. We take the coupling constant χ to be proportional to $\hbar\Omega$ and, to leading order, to decrease with the total number of HO excitations, as shown by Rowe [48] based on self-consistent arguments.

The NCSpM outcome reveals a quite remarkable agreement with the experiment and *ab initio* results (Figure 4) [21]. Energies and eigenstates for ^{12}C were calculated for $\hbar\Omega = 18$ MeV given by the empirical estimate $\approx 41/A^{1/3} = 17.9$ MeV. The results are shown for $N_{\text{max}} = 20$, which we found sufficient for convergence. This N_{max} model space is further reduced by selecting the five most relevant symplectic irreps, extended up through $N_{\text{max}} = 20$ (6.6×10^3 positive-parity basis states). In comparison to experiment (Figure 4), the outcome for $\gamma = -1.71 \times 10^{-4}$ reveals that the lowest 0^+ , 2^+ , and 4^+ states of the $0p$ - $0h$ symplectic irreps closely reproduce the *g.st.* rotational band, while the lowest 0^+ states of the $4\hbar\Omega$ $4p$ - $4h$ (12 0) and the $2\hbar\Omega$ $2p$ - $2h$ (6 2) irreps are found to lie close to the Hoyle state and the 10-MeV 0^+ resonance, respectively. The NCSpM successfully reproduces the 3^- state by the $1\hbar\Omega$ (3 3), as well as other observables, such as mass rms radii, electric quadrupole moments and $B(E2)$ transition strengths (Figure 4). The model is also applicable to the low-lying states of ^8Be and *sd*-shell nuclei without any adjustable parameters [22, 45]. This suggests that the fully microscopic NCSpM model has indeed captured an important part of the underlying physics and informs key features of the interaction and structure primarily responsible for the formation of such simple patterns.

4 Alpha-Capture Reactions of Interest to X-Ray Burst Nucleosynthesis

Surface α -clustering can be quantified using a spectroscopic amplitude, which is calculated, in the center-of-mass frame, as the overlap between the wave function of ^{20}Ne and the cluster wave function, with the α -particle $|\psi_{\alpha_c}\rangle$ at a distance a from the ^{16}O nucleus $|\psi_{A_c}\rangle$, written symbolically as:

$$u_l(r) = \langle \psi_{20\text{Ne}} | \mathcal{A} \{ |\psi_{A_c}\rangle \times |\psi_{\alpha_c}\rangle \} \times Y_{l0}(\hat{a}) \frac{\delta(r-a)}{ra}. \quad (2)$$

By expanding the δ -function in the orthonormal HO basis and the ^{20}Ne wave-function in the symplectic basis (with coefficients determined either from the SA-NCSM or NCSpM), the spectroscopic amplitudes are calculated using the overlaps between the symplectic basis states and the cluster states. These overlaps, for the stretched symplectic states, can be calculated using a recursive formula [49], which shows a direct correspondence between the $2\hbar\Omega$ $1p$ - $1h$ symplectic excitation induced by the symplectic raising operator and a $2\hbar\Omega$ excitation in the relative motion of the clusters. The usual spectroscopic factors are

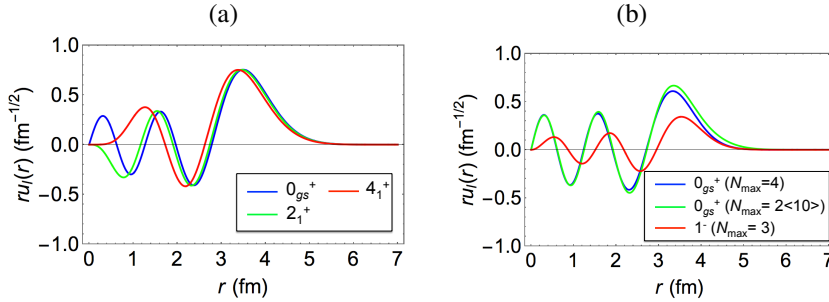


Figure 5. (color online) Spectroscopic amplitudes for (a) the ground-state rotational band (0_{gs}^+ , 2_1^+ , and 4_1^+), using in the NCSpm wave functions, and (b) for the ground state (in $N_{\text{max}} = 4$ and $\langle 2 \rangle 10$ model spaces) and 1_1^- state (in $N_{\text{max}} = 3$ model space), using *ab initio* SA-NCSM wave functions. Results are limited to a single irrep and stretched symplectic states.

calculated from the amplitude as,

$$S_\alpha = \int_0^\infty dr r^2 |u_l(r)|^2. \quad (3)$$

We calculate spectroscopic amplitudes for the ^{20}Ne ground-state rotational band and 1_1^- state (Figure 5). We note that the 1_1^- state is still not converged in this comparatively small model space; nonetheless, we expect that a larger model space $N_{\text{max}} = \langle 1 \rangle 11$ will result in a slightly higher peak and longer tail, as observed for the ground state as one goes from the $N_{\text{max}} = 4$ model space to the larger $\langle 2 \rangle 10$ model space (Figure 5b). There are two major indicators for clustering, which are best used in conjunction with one another: an enhanced spectroscopic amplitude near the touching distance between the clusters, and a large spectroscopic factor. We find an enhancement of the spectroscopic amplitude for the low-lying 1_1^- state of ^{20}Ne closer to the surface as compared to the ground state and its rotational band. Notably, the spectroscopic factor for the 1_1^- state is considerably larger than that seen for the 0^+ , 2^+ , and 4^+ states. This is indicative of the formation of the $^{16}\text{O} + \alpha$ structure in the 1_1^- state, which lies very close to the α -threshold.

From the spectroscopic amplitude for the 1_1^- state, the alpha-decay width is calculated using an R -matrix expression $\Gamma_\alpha = 2P_L\gamma_L^2$. The reduced width $\gamma_L = \sqrt{\frac{\hbar^2 R}{2\mu}} u_l(a)$ is dependent on the spectroscopic amplitude at the channel radius a and the reduced mass μ , and the barrier penetrability P_L is given by $P_L(a) = \frac{k a}{H_L^+(\eta, k a)}$, where k is the relative momentum of the alpha-particle, $H_L^+(\eta, k r)$ are the spherical Coulomb-Hankel functions, and $\eta = \frac{Z_1 Z_2 e^2 \mu}{\hbar^2 k}$ is the Sommerfeld parameter. The alpha-decay width is, in turn, used to calculate the reaction rate for the $^{16}\text{O}(\alpha, \gamma)^{20}\text{Ne}$ reaction through the 1_1^- resonance as a

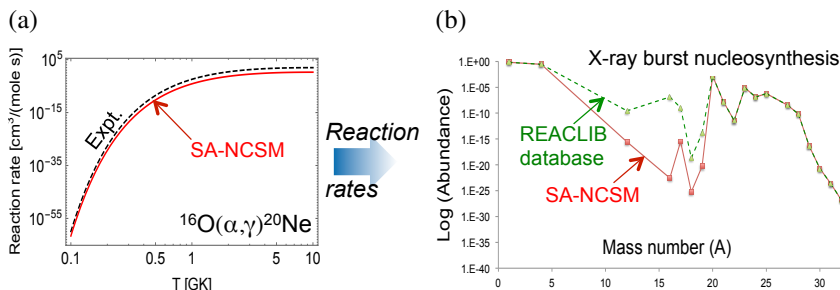


Figure 6. (color online) (a) Reaction rates calculated from the *ab initio* $N_{\max}=(2)10$ SA-NCSM ^{20}Ne density for the 1^- state. (b) Effect on the abundance pattern from X-ray burst (XRB) nucleosynthesis simulations (based on X_{net} [50]) when calculated reaction rates are used as compared to present systematics, for fixed astrophysical conditions.

function of the astrophysical T_9 temperature (Figure 6a). For X-ray burst (XRB) temperatures (~ 1 GK) the Gamow window peaks right around the 1.3-MeV 1^- resonance state, and hence the reaction rate is dominated by the contribution through this channel at these astrophysical temperatures. The reaction rate is supplied to XRB nucleosynthesis simulations, based on X_{net} [50], and the abundance pattern is obtained from the SA-NCSM calculated alpha width (Figure 6b). Compared to the present JINA Reaclib database, for fixed astrophysical conditions, the calculations show good agreement for $A > 20$. They also show the need for complete *R*-matrix calculations, which include excitations of the clusters and the interplay of the near 3^- resonance. The present calculations provide the first step toward a more complete treatment, and are especially important for the intermediate-mass region. In particular, reaction rates are currently based on the predictions of the Hauser-Feshbach theory, which assumes high level densities, but for the intermediate-mass region and the astrophysically relevant energies, the reaction rates are expected to be governed by low level densities and dominated by a few isolated resonances. This includes short-lived nuclei with sparse experimental data that are difficult, and often impossible, to be measured.

5 Exact Isovector Pairing in a Shell Model Framework

For the nuclei under consideration, we explore the formation of like-nucleon and proton-neutron (pn) isovector pairs together with pn isoscalar correlations, of importance to two-nucleon correlations in break-up reaction channels. These investigations are carried forward in the framework of exact pairing in a shell model with non-degenerate single-particle energies (s.p.e.) that are empirically derived (in general, they can also be determined in a mean-field approach, including density functional theory for heavy nuclei, and in a spherical shell

model). The method provides, for the first time, exact solutions when non-degenerate s.p.e. and the challenging pn correlations are considered, based on recent mathematical developments [51, 52]. Results for light up through medium-mass nuclei ($10 \leq A \leq 62$) are found to remarkably agree with experiment [53] (see Figure 7 for selected p - and sd -shell nuclei including the deformed ^{20}Ne). The outcome suggests that enhanced deformation does not preclude pair formation – indeed, collective modes appear to remain dominant even in the presence of pairing (see also [54, 55]), while the most noticeable effect of the latter is typically in reducing the moment of inertia.

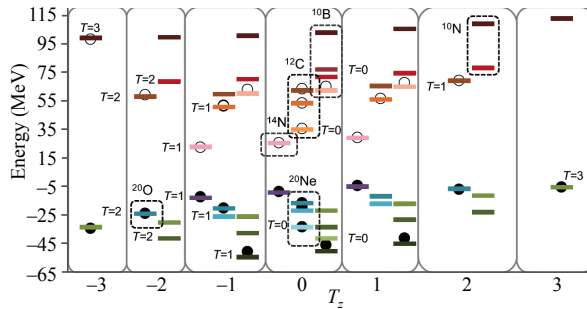


Figure 7. (color online) Exact solutions (lines) for a pairing Hamiltonian with experimentally deduced non-degenerate single-particle energies, like-nucleon and proton-neutron isovector pairing, proton-neutron isoscalar term, and a Coulomb potential, as compared to experimental 0^+ states (circle).

In short, we have demonstrated the emergence of orderly patterns in nuclei from first principles, with associated hidden symmetry exploited, in turn, in the SA-NCSM and the NCSpM. We have illustrated the efficacy of the NCSpM to gain new insights into the microscopic structure of nuclei, as well as into cluster-like and pairing correlations. We have studied the $\alpha + ^{16}\text{O}$ capture reaction through the 1^- resonance as a first example for alpha capture reactions in the intermediate-mass region of importance to x-ray burst nucleosynthesis simulations.

Acknowledgments

We thank D. Rowe, J. Wood, G. Rosensteel, and J. E. Escher for useful discussions. This work was supported by the U.S. NSF (OIA-1738287, ACI - 1713690), SURA, and the Czech SF (16-16772S), and benefitted from computing resources provided by Blue Waters, LSU (www.hpc.lsu.edu), and the National Energy Research Scientific Computing Center (NERSC). Part of this work was performed under the auspices of the DOE by Lawrence Livermore National Laboratory under Contract No. DE-AC52-07NA27344, with support from the U.S. Department of Energy, Office of Science, Office of Workforce

Ab Initio Picture of Nuclei: Shapes, Rotations, and Vibrations

Development for Teachers and Scientists, Office of Science Graduate Student Research (SCGSR) program, and from LLNL's LDRD program (16-ERD-022). The SCGSR program is administered by the Oak Ridge Institute for Science and Education (ORISE) for the DOE. ORISE is managed by ORAU under contract number DE-SC0014664.

References

- [1] P. Navrátil, J.P. Vary, and B.R. Barrett (2000) *Phys. Rev. Lett.* **84** 5728.
- [2] S.C. Pieper, K. Varga, and R.B. Wiringa (2002) *Phys. Rev. C* **66** 044310.
- [3] M. Wloch, D.J. Dean, J.R. Gour, M. Hjorth-Jensen, K. Kowalski *et al.* (2005) *Phys. Rev. Lett.* **94** 212501.
- [4] G. Hagen, T. Papenbrock, D.J. Dean, and M. Hjorth-Jensen (2008) *Phys. Rev. Lett.* **101** 092502.
- [5] A.F. Lisetskiy, B.R. Barrett, M.K.G. Kruse, P. Navrátil, I. Stetcu, and J.P. Vary (2008) *Phys. Rev. C* **78** 044302.
- [6] P. Navrátil, S. Quaglioni, I. Stetcu, and B.R. Barrett (2009) *J. Phys. G: Nucl. Part.* **36** 083101.
- [7] R. Roth and P. Navrátil (2007) *Phys. Rev. Lett.* **99** 092501.
- [8] E. Epelbaum, H. Krebs, D. Lee, and U.G. Meissner (2011) *Phys. Rev. Lett.* **106** 192501.
- [9] K. Tsukiyama, S.K. Bogner, and A. Schwenk (2011) *Phys. Rev. Lett.* **106** 222502.
- [10] T. Dytrych, K.D. Launey, J.P. Draayer, P. Maris, J.P. Vary *et al.* (2013) *Phys. Rev. Lett.* **111** 252501.
- [11] T. Abe, P. Maris, T. Otsuka, N. Shimizu, Y. Utsuno, and J. Vary (2012) *Phys. Rev. C* **86** 054301.
- [12] A. Cipollone, C. Barbieri, and P. Navrátil (2013) *Phys. Rev. Lett.* **111** 062501.
- [13] C. Romero-Redondo, S. Quaglioni, P. Navrátil, and G. Hupin (2014) *Phys. Rev. Lett.* **113** 032503.
- [14] J.L. Wood (2017) *Emergent phenomena in atomic nuclei from large-scale modeling: a symmetry-guided perspective* ed. K D Launey (World Scientific Publishing Co.) ISBN 978-981-3146-04-4.
- [15] D.J. Rowe and J.L. Wood (2010) *Fundamentals of nuclear models: foundational models* (World Scientific, Singapore).
- [16] G. Rosensteel and D.J. Rowe (1977) *Phys. Rev. Lett.* **38** 10.
- [17] D.J. Rowe (1985) *Rep. Progr. Phys.* **48** 1419.
- [18] M. Harvey (1968) *Adv. Nucl. Phys.* **1** 67.
- [19] J.P. Elliott and M. Harvey (1962) *Proc. Roy. Soc. A* **272** 557.
- [20] D. Rowe (2013) *AIP Conf. Proc.* **1541** 104.
- [21] A.C. Dreyfuss, K.D. Launey, T. Dytrych, J.P. Draayer, and C. Bahri (2013) *Phys. Lett. B* **727** 511.
- [22] G.K. Tobin, M.C. Ferriss, K.D. Launey, T. Dytrych, J.P. Draayer, and C. Bahri (2014) *Phys. Rev. C* **89** 034312.
- [23] A.C. Dreyfuss, K.D. Launey, T. Dytrych, J.P. Draayer, R.B. Baker, C.M. Deibel, and C. Bahri (2017) *Phys. Rev. C* **95** 044312.

- [24] K.D. Launey, T. Dytrych, and J.P. Draayer (2016) *Prog. Part. Nucl. Phys.* **89** 101.
- [25] D.J. Rowe, G. Thiamova, and J.L. Wood (2006) *Phys. Rev. Lett.* **97** 202501.
- [26] J. Draayer, K. Weeks, and G. Rosensteel (1984) *Nucl. Phys.* **A419** 1.
- [27] J. Escher and J.P. Draayer (1999) *Phys. Rev. Lett.* **82** 5221.
- [28] M. Jarrío, J.L. Wood, and D.J. Rowe (1991) *Nucl. Phys. A* **528** 409.
- [29] C. Bahri and D.J. Rowe (2000) *Nucl. Phys. A* **662** 125.
- [30] J.P. Elliott (1958) *Proc. Roy. Soc. A* **245** 128.
- [31] J.P. Elliott (1958) *Proc. Roy. Soc. A* **245** 562.
- [32] C. Bahri, J. Draayer, and S. Moszkowski (1992) *Phys. Rev. Lett.* **68** 2133.
- [33] A. Zuker, J. Retamosa, A. Poves, and E. Caurier (1995) *Phys. Rev. C* **52** R1741.
- [34] T. Dytrych, K.D. Sviratcheva, J.P. Draayer, C. Bahri, and J.P. Vary (2008) *J. Phys. G* **35** 123101.
- [35] A. Shirokov, J. Vary, A. Mazur, and T. Weber (2007) *Phys. Lett. B* **644** 33.
- [36] D.R. Entem and R. Machleidt (2003) *Phys. Rev. C* **68** 041001.
- [37] T. Dytrych, K.D. Launey, and J.P. Draayer (2014) *Symmetry-adapted no-core shell model* (McGraw-Hill).
- [38] A. Ekström, G. Baardsen, C. Forssén, G. Hagen, M. Hjorth-Jensen, G.R. Jansen, R. Machleidt, W. Nazarewicz et al. (2013) *Phys. Rev. Lett.* **110** 192502.
- [39] F. Hoyle 1954 *Astrophys. J. Suppl. Ser.* **1** 121.
- [40] M. Chernykh, H. Feldmeier, T. Neff, P. von Neumann-Cosel, and A. Richter (2007) *Phys. Rev. Lett.* **98** 032501.
- [41] D.T. Khoa, D.C. Cuonga, and Y. Kanada-En'yo (2011) *Phys. Letts. B* **695** 469.
- [42] H.O.U. Fynbo et al. (2005) *Nature* **433** 136.
- [43] M. Freer et al. (2009) *Phys. Rev. C* **80** 041303.
- [44] W.R. Zimmerman et al. (2013) *Phys. Rev. Lett.* **110** 152502.
- [45] K.D. Launey, T. Dytrych, J.P. Draayer, G.K. Tobin, M.C. Ferriss et al. (2013) *Proceedings of the 5th International Conference on "Fission and properties of neutron-rich nuclei", ICFNS, November 4 - 10, 2012, Sanibel Island, Florida* ed Hamilton J H and Ramayya A V (World Scientific, Singapore) p 29.
- [46] K.D. Launey, A.C. Dreyfuss, J.P. Draayer, T. Dytrych, and R.B. Baker (2014) *J. Phys.: Conf. Ser.* **569** 012061.
- [47] G. Rosensteel and J.P. Draayer (1985) *Nucl. Phys. A* **436** 445.
- [48] D.J. Rowe (1967) *Phys. Rev.* **162** 866.
- [49] Y. Suzuki (1986) *Nucl. Phys. A* **448** 395.
- [50] W. Hix and F.K. Thielemann (1999) *J. Comput. Appl. Math.* **109** 321.
- [51] X. Guan, K.D. Launey, M. Xie, L. Bao, F. Pan, and J.P. Draayer (2012) *Phys. Rev. C* **86** 024313.
- [52] F. Pan and J.P. Draayer (2002) *Phys. Rev. C* **66** 044314.
- [53] M.E. Miora, K.D. Launey, D. Kekejian, F. Pan, and J.P. Draayer (2015) *APS Conference, DNP, Santa Fe, NM, 28-31 October 2015* <http://meetings.aps.org/Meeting/DNP15/Session/EA.80>
- [54] C. Bahri, J. Escher, and J. Draayer (1995) *Nucl. Phys. A* **592** 171.
- [55] F. Pan, X. Ding, K.D. Launey, H. Li, X. Xu, and J.P. Draayer (2016) *Nucl. Phys. A* **947** 234.